Scientific Research Publishing

Journal of Computer and Communications, 2025, 13(6), 217-233
https://www.scirp.org/journal/jcc
ISSN Online: 2327-5227
ISSN Print: 2327-5219

GNSS-R Soil Salinity Inversion Method Based on Multimodal Low-Rank Fusion Algorithm Using Tianmu-1 Satellite Data

Dongmei Song[1], Xianjun Wang[1], Mei Yong[2], Summiya Erdenesukh[3], Yuhai Bao[2], Bin Wang[1]

[1]College of Oceanography and Space Informatics, China University of Petroleum (East China), Qingdao, China
[2]College of Geographical Sciences, Inner Mongolia Normal University, Hohhot, China
[3]National University of Mongolia (NUM), Ulaanbaatar, Mongolia
Email: songdongmei@upc.edu.cn, s23160016@s.upc.edu.cn, yongmei2012@imnu.edu.cn, erdenesukh@num.edu.mn, baoyuhai@imnu.edu.cn, wangbin007@upc.edu.cn

How to cite this paper: Song, D.M., Wang, X.J., Yong, M., Erdenesukh, S., Bao, Y.H. and Wang, B. (2025) GNSS-R Soil Salinity Inversion Method Based on Multimodal Low-Rank Fusion Algorithm Using Tianmu-1 Satellite Data. *Journal of Computer and Communications*, **13**, 217-233.
https://doi.org/10.4236/jcc.2025.136015

Received: May 18, 2025
Accepted: June 27, 2025
Published: June 30, 2025

Abstract

Soil salinization is a critical global issue that constrains agricultural productivity and the sustainable development of ecological environments. Efficient and accurate monitoring of soil salinity is, therefore, of great significance. As an emerging passive remote sensing technology, Global Navigation Satellite System Reflectometry (GNSS-R) offers advantages such as all-weather, all-day capability and high spatiotemporal resolution, demonstrating broad application potential in soil parameter monitoring. Meanwhile, deep learning methods, with their powerful feature representation and modeling capabilities, have become essential tools in remote sensing inversion tasks. In this study, the Yellow River Delta is selected as the research area, and a multimodal low-rank fusion network model, MLF-Net, is proposed for high-precision soil salinity inversion based on GNSS-R data from the Tianmu-1 satellite. The results show that MLF-Net achieves a correlation coefficient of 0.9137 and a root mean square error (RMSE) of 0.8050 g/kg, outperforming comparison methods including Transformer, XGBoost, and artificial neural networks (ANN), in terms of both accuracy and stability. This study validates the feasibility and advantages of combining GNSS-R technology with deep learning approaches for soil salinity inversion, providing technical support and practical reference for saline-alkali land monitoring and precision agriculture.

Keywords

Tianmu-1, GNSS-R, Soil Salinity, Transformer

1. Introduction

Soil salinity, defined as the concentration of soluble salts in soil, is a key physical parameter that reflects the degree of soil salinization. Soil salinization is one of the primary causes of land degradation and desertification, particularly in irrigated farmland, grasslands in arid and semi-arid regions, and coastal wetlands, where the phenomenon is especially pronounced. It poses a major threat to global food security and is a critical factor contributing to land degradation. Therefore, effective monitoring of soil salinity is of great necessity.

Soil salinity can be obtained through *in situ* observations and remote sensing techniques. *In situ* measurements provide high-accuracy soil salinity data, but are time-consuming and labor-intensive, making them unsuitable for large-scale salinization monitoring. Optical remote sensing missions (such as MODIS and Landsat) offer relatively high spatial and temporal resolution for soil salinity monitoring; however, optical sensors are limited in their ability to directly sense surface soil properties, have poor penetration capabilities, and are significantly affected by weather conditions. Compared to optical methods, microwave remote sensing has the advantages of all-weather capability and the ability to penetrate vegetation, making it an effective approach for monitoring soil salinity. Existing research has mainly focused on active microwave remote sensing, and synthetic aperture radar (SAR) imagery has been demonstrated as an effective tool for detecting salinization. However, active microwave systems suffer from issues such as geometric distortions, complex noise, and limited temporal resolution, making it difficult to achieve high spatiotemporal resolution and high-precision soil salinity retrieval.

To overcome these limitations, Global Navigation Satellite System Reflectometry (GNSS-R) has emerged as a promising alternative for soil salinization monitoring. GNSS-R is characterized by its all-weather observation capability, high spatiotemporal coverage, and low cost, and has been widely applied in various remote sensing fields such as soil moisture estimation [1], ocean altimetry [2], and sea surface wind speed retrieval [3]. In recent years, with the advancement of multi-constellation GNSS systems, the potential of GNSS-R for soil parameter inversion has become increasingly evident, making it a growing focus of research in the remote sensing community.

Currently, spaceborne GNSS-R soil salinity retrieval methods can be broadly categorized into two approaches: physical modeling and data-driven methods. Physical modeling approaches are typically based on radar scattering models or electromagnetic wave propagation theory, utilizing surface reflectivity and Fresnel reflection coefficients to estimate soil salinity. These methods are grounded in well-established physical principles and offer strong interpretability. However, they often exhibit limited modeling capability under complex surface conditions and rely heavily on prior information.

In contrast, data-driven methods—particularly those based on machine learning—construct nonlinear mapping relationships between observational data and

target variables. These methods exhibit strong feature learning and adaptive capabilities, enabling high-accuracy retrieval without the need for precise physical modeling, and are well-suited for heterogeneous and dynamic surface environments. Traditional machine learning-based approaches for soil salinity retrieval often rely on input features derived from physical calculations, such as surface Fresnel reflectivity. However, such features are typically single-value indicators derived from simplified models and may fail to capture the complex scattering information embedded in GNSS-R observations.

By contrast, the Delay-Doppler Map (DDM), a two-dimensional power distribution of the original GNSS-R observation, retains the full spatiotemporal structure of the signal. Directly using the DDM image as model input allows deep learning models to automatically extract high-dimensional information such as scattering patterns, intensity distributions, and multipath structures. This significantly enhances the model's representational capacity and generalization ability for soil salinity retrieval. Furthermore, DDM images are highly sensitive to changes in surface electrical conductivity, which can help the model better characterize the spatial heterogeneity of soil salinity. To further strengthen the model's ability to capture structural information in DDM images, this study introduces Tucker decomposition to perform tensor-based dimensionality reduction while retaining the original DDM input. This approach mitigates the redundancy and noise present in raw DDM data to some extent, contributing to improved model stability and generalization performance.

At present, most studies still rely on convolutional neural networks (CNNs) to extract features from DDM images [4]. While CNNs are effective in capturing local spatial features, they primarily rely on local convolutional kernels, making it difficult to model the global contextual information in DDM images. However, global structures are of critical importance in characterizing surface scattering properties.

In recent years, with the rapid advancement of Transformer architectures in natural language processing (NLP) and computer vision (CV) [5], Transformers have demonstrated remarkable advantages in modeling long-range dependencies, enabling parallel computation, offering architectural flexibility, and achieving superior performance across a wide range of tasks. Compared to CNNs, Transformers can effectively capture long-range dependencies through global attention mechanisms, thereby overcoming the limitations of CNNs in terms of receptive field size and global structure modeling. These characteristics make Transformers better suited for extracting spatial structures and scattering features embedded in DDM images.

To address the aforementioned challenges, this study proposes a GNSS-R soil salinity inversion method based on a Multimodal Low-Rank Fusion Network (MLF-Net). The proposed approach utilizes DDM images along with auxiliary parameters such as surface reflectivity as multimodal inputs. By incorporating low-rank constraints and a fusion mechanism, the model enables efficient and collab-

orative modeling of multi-source features.

The remainder of this paper is organized as follows. Section 2 introduces the study area, and the datasets used. Section 3 provides a detailed description of the proposed method. Section 4 presents experimental results and analysis. Finally, Section 5 concludes the study.

2. Datasets

In this study, the Yellow River Delta region was selected as the study area. The primary data source is GNSS-R observations from the Tianmu-1 satellite. In addition, auxiliary soil parameters such as bulk density and soil moisture content were obtained from the Soil Moisture Active Passive (SMAP) mission dataset.

2.1. Study Area Overview

This study focuses on the high-efficiency economic and ecological zone of the Yellow River Delta (116˚55'E-120˚19'E, 36˚25'N-38˚14'N), hereinafter referred to as the Yellow River Delta region. As a representative coastal saline-alkali area, the Yellow River Delta has approximately 442,900 hectares of salinized soil, accounting for about 50% of the region's total area [6]. Therefore, in light of China's national strategy for ecological protection and high-quality development in the Yellow River Delta, there is an urgent need for a precise and reliable remote sensing method for soil salinity inversion. Such a method would provide critical data support for regional ecological conservation and the improvement of agricultural productivity [7].

2.2. Data Description

Tianmu-1 Satellite Constellation. Operated by Aerospace Tianmu (Chongqing) Satellite Technology Co., Ltd.—a subsidiary of CASIC—the Tianmu-1 constellation is China's first commercial low-Earth-orbit meteorological satellite system. Its inaugural satellite ("Tianmu-1 00") was launched on 14 October 2021. As of this study, 23 satellites are in orbit, each carrying GNSS occultation and reflection payloads that simultaneously support five navigation systems: GPS, BeiDou (BDS), Galileo (GAL), GLONASS (GLO), and QZSS [8]. This multi-constellation capability greatly enhances global atmospheric data acquisition, enabling all-weather retrieval of atmospheric, land-surface, and oceanic parameters. This study utilizes Level-1 reflected signal data from the GNSS-R instrument onboard the Tianmu-1 satellite for the months of May, June, July, and September. The Tianmu-1 dataset provides Delay-Doppler Maps (DDMs) and a set of single-feature parameters.

In addition, this study incorporates two auxiliary datasets: the Soil Moisture Active Passive (SMAP) mission and the Harmonized World Soil Database 2.0 (HWSD 2.0) [9], to provide supplementary parameters. The SMAP data product used is the Enhanced Level-3 dataset [10], with a grid resolution of 9 km × 9 km and stored in HDF5 format. SMAP offers a variety of environmental variables,

including vegetation optical depth, surface roughness coefficient, land surface temperature, vegetation water content, soil bulk density, soil clay fraction, and soil moisture content. Among these, soil moisture is used as the reference variable, while the remaining parameters are treated as individual input features.

The HWSD 2.0 dataset provides the soil sand fraction, which serves as an additional auxiliary input. The complete list of auxiliary features used in this study is summarized in **Table 1**.

Table 1. Summary of auxiliary features.

Data sources	Feature representation	Feature name
Tianmu-1	SR_Corr	Corrected Surface Reflectivity
	Angle	Incidence Angle
	DDMA	Mean of DDM
	Peak	Peak of DDM
	SNR	Signal-to-Noise Ratio
	ROW	Row of DDM Peak
	COL	Column of DDM Peak
	Time	Satellite Observation Time
	Lon	Longitude
	Lat	Latitude
SMAP	VOD	Vegetation Optical Depth
	VWC	Surface Water Content
	Tem	Surface Temperature
	Rough	Surface Roughness
	Bulk	Soil Bulk Density
	Clay	Soil Clay Fraction
HWSD2.0	Sand	Soil Sand Fraction

2.3. Data Preprocessing

First, standard quality control procedures were applied to filter the observational data. Tianmu-1 observations with incidence angles greater than 65˚ were excluded. Data with receiver antenna gain less than 0 dB were removed, and only observations with signal-to-noise ratio (SNR) between 0 and 14 were retained. From the filtered dataset, feature sets correlated with soil salinity were extracted as inputs to the model. The input features consist of two parts: DDM images and auxiliary features.

Previous studies have demonstrated a strong correlation between surface reflectivity and soil salinity. Since most land surfaces are relatively smooth, GNSS-R signals are primarily composed of coherent reflections. Under this assumption,

surface reflectivity can be calculated based on Equation (1).

$$\Gamma_{surface}(\theta_i) = \frac{P_r (R_{ts} + R_{sr})^2 (4\pi)^2}{P_t G_t G_r \lambda^2} \tag{1}$$

In the equation, P_r denotes the power at the peak point of the DDM image; P_t is the transmitted power of the transmitter; G_t represents the transmitter antenna gain; R_{ts} is the distance between the transmitter and the specular reflection point; R_{sr} is the distance between the specular reflection point and the receiver; G_r denotes the receiver antenna gain; λ is the wavelength of the GNSS navigation satellite signal (0.19 m);and $\Gamma_{surface}(\theta_i)$ represents the surface reflectivity at the incidence angle θ_i.

After converting all terms into decibel (dB) scale, the surface reflectivity P_r can be calculated using the following Equation (2):

$$\begin{aligned}\Gamma_{surface}(\theta_i) &= 10\log P_r + 20\log(R_{ts} + R_{sr}) + 20\log 4\pi \\ &-10\log P_t - 10\log G_t - 10\log G_r - 20\log\lambda\end{aligned} \tag{2}$$

The surface reflectivity derived from the bistatic radar equation is affected by factors such as surface roughness and vegetation attenuation. Therefore, it is essential to correct the surface reflectivity for vegetation attenuation and surface roughness effects.

In this study, we adopt the parameterized tau-omega model proposed by Bindlish and Barros [11], which integrates vegetation water content data provided by the SMAP Level-3 product to mitigate the influence of vegetation on surface reflectivity. The tau-omega model accounts for the incoherent combination of vegetation and underlying soil contributions. Assuming that the scattering effect of vegetation can be neglected, the corresponding formulation of the tau-omega model is given as follows:

$$\sigma_{soil} = (\Gamma_{surface}^{0.5} - \sigma_{\text{veg}})^2 \big/ \tau^2 \tag{3}$$

$$\tau = \exp(-B \bullet vwc \bullet \sec(\theta_i)) \tag{4}$$

$$\sigma_{\text{veg}} = A \bullet vwc \bullet \cos(\theta) \bullet (1 - \tau^2) \tag{5}$$

In the above equation, $\Gamma_{surface}$ represents the surface reflectivity calculated from Equation (2); σ_{veg} denotes the scattering contribution from vegetation; σ_{soil} refers to the scattering contribution from the soil layer; τ^2 is the two-way vegetation transmissivity; vwc is the vegetation water content extracted from the SMAP dataset; and θ_i is the satellite incidence angle. Parameters A and B are empirical coefficients related to vegetation density and two-way propagation path, respectively. In this study, we adopt generally applicable values for all land cover types, where A = 0.0012 and B = 0.091. The final corrected surface reflectivity σ_{soil}^2 is obtained after adjusting for vegetation attenuation.

Meanwhile, it is also necessary to correct for surface roughness. In this study, the surface reflectivity is further adjusted using the surface roughness coefficient obtained from the SMAP dataset, as follows:

$$\Gamma_{rough} = \sigma_{soil}^2 \bullet \exp(-h\cos^2\theta) \tag{6}$$

In the equation, the exponential term represents the signal attenuation caused by surface roughness; h denotes the surface roughness coefficient obtained from the SMAP dataset; Γ_{rough} is the surface reflectivity further corrected for surface roughness h. The corrected reflectivity serves as an input feature to the network model, enabling a better representation of soil salinity variations.

3. Proposed Method

3.1. Model Construction

To effectively capture the interactive relationships between DDM images and auxiliary features [12], and to thoroughly explore the latent physical information contained in DDM images, this study proposes a Multimodal Low-Rank Fusion Network (MLF-Net), as illustrated in **Figure 1**. MLF-Net consists of three main components: the T-ResCANet module, the HybridFormer module, and the feature fusion module.

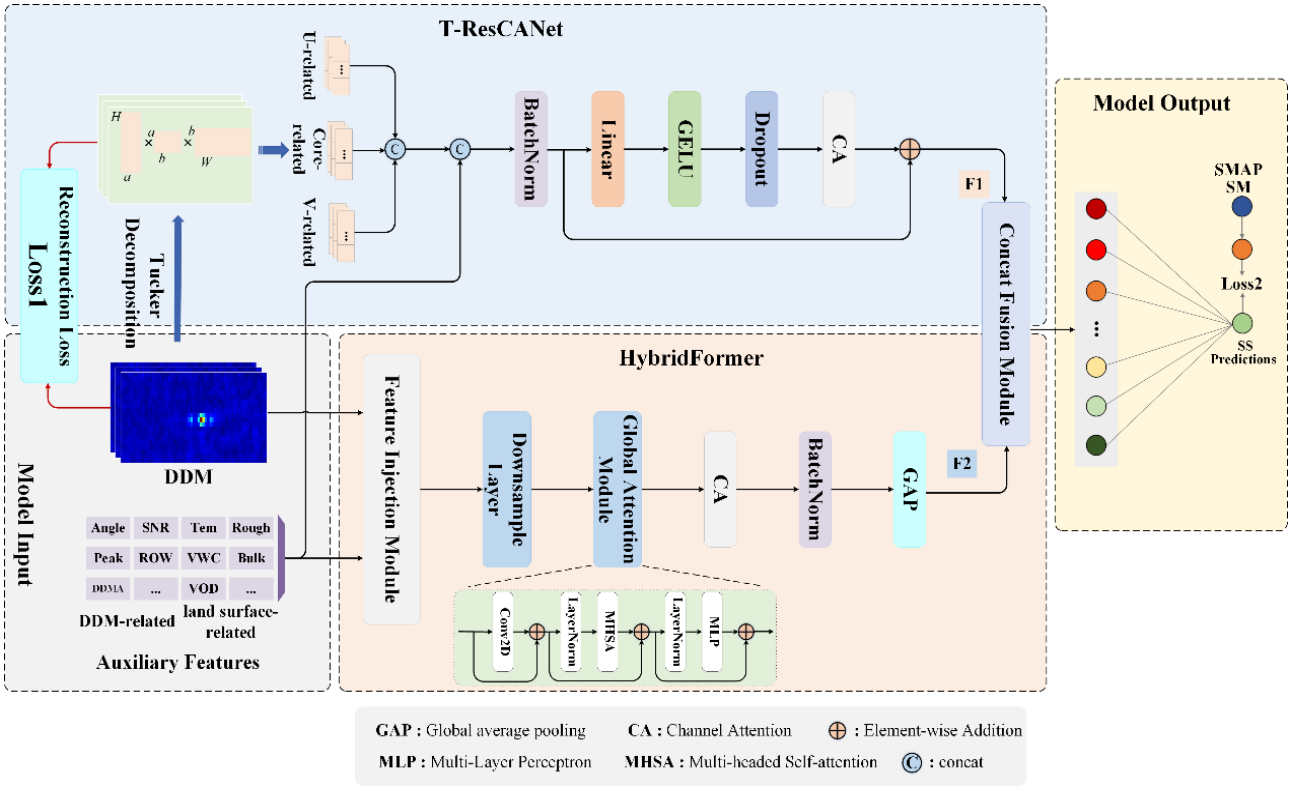

Figure 1. Multimodal low-rank fusion network (MLF-Net).

The T-ResCANet module integrates physical prior features extracted from auxiliary data such as surface reflectivity with physical structural information of DDM images obtained through Tucker tensor decomposition, resulting in fused latent physical features. The HybridFormer module employs a Transformer architecture combined with channel attention to model the global structural distribution of the

two-dimensional fused image, extracting spatial structural features from the fused 2D representation. The feature fusion module then combines the information from these two components, and the final soil salinity estimate is obtained through a fully connected layer.

The T-ResCANet module primarily performs Tucker low-rank decomposition on the DDM images to extract relevant statistical features from the core tensor and factor matrices. This process effectively reduces redundant feature dimensions while preserving the structural information of the images. The low-rank features are concatenated with auxiliary features and then fed into a residual network composed of batch normalization layers, linear mappings, nonlinear activations, dropout layers, and a channel attention (CA) module, which possesses strong feature transformation and regularization capabilities. This module enhances key responses related to soil salinity in the compressed feature space. The resulting feature $F1$ serves as the output of the T-ResCANet branch. Additionally, to ensure the effectiveness of the Tucker decomposition, a reconstruction loss $Loss1$ is introduced as an auxiliary supervision signal.

The Tucker low-rank decomposition module decomposes the DDM image $\mathcal{X} \in \mathbb{R}^{20\times 61}$ into a core tensor $\mathcal{G} \in \mathbb{R}^{4\times 6}$ and two factor matrices $U \in \mathbb{R}^{20\times 4}$, $V \in \mathbb{R}^{6\times 61}$ according to Equation (7). Subsequently, statistical measures of the core tensor—including mean, standard deviation, L2 norm, maximum, and minimum—are computed to capture the core distribution characteristics. Statistical measures of the factor matrices are also calculated along the columns, including mean, standard deviation, and L2 norm, to analyze feature variations of the DDM along different dimensions. Furthermore, singular value decomposition (SVD) is introduced to extract principal component information, aiding in identifying the most significant patterns within the data and enhancing the representativeness of the features. The extracted statistics are finally concatenated into a one-dimensional feature vector, which is then fused with the auxiliary features.

It is worth noting that since the reconstruction loss inherently reflects the fitting degree of the low-rank representation to the original DDM data and helps strengthen the recognition of boundary and outlier samples, this reconstruction loss is incorporated as part of the overall loss function in the proposed method.

$$\mathcal{X} \approx U \times_1 \mathcal{G} \times_2 V \tag{7}$$

The HybridFormer module aims to extract deep features with both local and global perception capabilities from the original DDM images and auxiliary features. It consists of three main components: A feature injection module that fuses the DDM image and auxiliary variables at the feature level by embedding the auxiliary features into the DDM image representations.; a multi-scale feature extraction module that sequentially applies down sampling, a global attention mechanism, and a channel attention (CA) mechanism to progressively capture deep representations relevant to soil salinity; and a compression module that reduces the high-dimensional features into a compact feature vector F2 via batch normalization and global average pooling (GAP). This design enables the module to effec-

tively learn long-range dependencies and semantic patterns from raw observations, facilitating the modeling of complex feature interactions essential for accurate soil salinity inversion.

The global attention module employs a convolutional layer as a positional embedding to inject spatial information into the subsequent attention mechanism. This is followed by layer normalization to standardize the input and enhance training stability. The core component is a multi-head self-attention mechanism designed to capture long-range dependencies and spatial correlations across the entire feature map. After the attention operation, a multilayer perception (MLP) is applied, and residual connections are utilized to ensure stable training.

The multi-head self-attention mechanism models relationships between arbitrary positions across the entire 2D fused input feature map X, formally expressed as:

$$Q = K = V = X \tag{8}$$

Here, Q denotes the query vector, which determines the content to be focused on within the attention mechanism. K represents the key vector, used to compute the correlation between Q and other positions in X, providing additional contextual information. V is the value vector that contains the positional information of each element in X.

For each attention head $i \in \{1, 2, ..., h\}$, the Q, K, and V vectors are projected into lower-dimensional spaces, resulting in:

$$Q_i = XW_i^Q \tag{9}$$

$$K_i = XW_i^K \tag{10}$$

$$V_i = XW_i^V \tag{11}$$

Here, W_i^Q, W_i^K and W_i^V denote the projection matrices for the i-th head. Within each head, the scaled dot-product attention is computed as follows:

$$head_i = Attention\left(Q_i, K_i, V_i\right) = softmax\left(\frac{Q_i K_i^T}{\sqrt{d_k}}\right)V \tag{12}$$

After computing the attention outputs of all heads, the results from each head are concatenated along the feature dimension and then projected back to the original dimension to obtain the final multi-head attention output:

$$MHSA\left(Q, K, V\right) = Concat\left(head_1, head_2, \cdots, head_h\right)W^O \tag{13}$$

Here, W^O denotes the output projection matrix, and *Concat* represents the concatenation operation along the feature dimension. This mechanism enables each position to dynamically adjust its attention to other positions while integrating global contextual information.

The Multilayer Perceptron (MLP) module consists of two linear transformation layers, a depth wise separable convolution layer, and a nonlinear activation function. This architecture is designed to perform linear mappings along the channel

dimension for each input feature, while simultaneously introducing local spatial awareness. The nonlinear activation enhances the model's representational capacity, thereby improving its ability to capture complex feature patterns.

The feature vectors *F*1 and *F*2 output from the two branches are fused and then fed into a final fully connected layer for soil salinity prediction. To improve the model's generalization ability and impose structural constraints, a joint loss function is adopted for optimization. The main loss term (*Loss*2) is the mean squared error (MSE) between the predicted soil salinity and the soil salinity derived from SMAP soil moisture data. The auxiliary loss term (*Loss*1) corresponds to the reconstruction error of the Tucker decomposition, which regularizes the low-rank tensor structure and prevents overfitting during feature extraction. The total loss function is formulated as follows:

$$\mathcal{L}_{\text{total}} = \mathcal{L}_2 + \lambda \mathcal{L}_1 = Loss2 + 0.1 \times Loss1 \tag{14}$$

The weighting coefficient $\lambda = 0.1$ controls the contribution of the auxiliary loss, effectively guiding the model to maintain interpretability and compactness of the input feature structure while ensuring prediction accuracy.

3.2. Hyperparameter Settings

The model inputs consist of DDM images and corrected reflectance auxiliary parameters. The dataset, constructed based on SMAP data, contains a total of 15,000 samples, with 80% of the data used for training. During training, the following hyperparameters are set: learning rate of 0.001; 100 epochs; batch size of 500; optimizer is AdamW; loss function is mean squared error (MSE); dropout rate is 0.1. The experiments are conducted using the PyTorch framework.

In this study, both the main loss (*Loss*2) and the auxiliary loss (*Loss*1) utilize the Mean Squared Error (MSE) as the loss function, which is a commonly used metric for numerical accuracy. The calculation formula is as follows:

$$L_{MSE} = \frac{1}{n}\sum_{i=1}^{n}(f_i - y_i)^2 \tag{15}$$

3.3. Model Training

In the microwave band, variations in soil moisture and salinity influence the soil's electrical conductivity, which in turn affects its dielectric constant. Therefore, soil dielectric models form the fundamental basis for microwave remote sensing inversion of soil moisture and salinity. The real part of the dielectric constant of saline soil is primarily controlled by soil moisture, while the imaginary part is jointly determined by moisture and salinity. Accordingly, this study employs soil salinity values derived from SMAP-provided soil moisture data through the *Wang* empirical model [13] and an improved *Dobson-S* model [14] as reference values for model training. The *Wang* empirical model and the improved *Dobson-S* model are expressed as follows:

$$\varepsilon = 3.1 + 17.36m_v + 63.12m_v^2 + j(0.031 + 4.65m_v + 20.42m_v^2) \tag{16}$$

$$S = \varepsilon'' \cdot \frac{2\pi\varepsilon_0}{A\zeta\chi} \cdot \frac{\rho_s}{(\rho_s - \rho_b)\rho_b} \cdot \frac{f}{m_v^{\beta''/\alpha-2}} \tag{17}$$

In the equations, the parameter A depends on the types of salt ions present in the soil; in this study, it is set to 0.78. ρ_b and ρ_s represent soil bulk density and particle density, respectively. f denotes the frequency, and ε_0 is the free-space conductivity ($8.854\times10^{-12} F/m$). The shape factor α is taken as 0.65. ζ is the first-order fitting coefficient relating soil solution conductivity to salinity, set to 0.14. χ is a temperature compensation coefficient, expressed by Equation (18). β'' is a correction factor accounting for the soil's sand and clay content, defined by Equation (19).

$$\chi = \exp\left(-\Delta\cdot(2.033\times10^{-2} + 1.266\times10^{-4}\Delta + 2.464\times10^{-6}\Delta^2)\right) \tag{18}$$

$$\beta'' = (133.797 - 0.603S - 1.66C)/100 \tag{19}$$

In the equations, $\Delta = 25 - T(^\circ C)$, $T(^\circ C)$ denotes the surface temperature; C represents the proportion of sand in the soil; and S represents the proportion of clay in the soil.

The test dataset was input into the trained model, and the inversion accuracy of the Multimodal Low-Rank Fusion Network (MLF-Net) was evaluated using two performance metrics: the correlation coefficient (*R*) and the root mean square error (*RMSE*). The correlation coefficient (*R*) measures the linear relationship between two variables, ranging from −1 to 1, where values closer to 1 indicate better model performance. The root mean square error (*RMSE*) is a commonly used metric to quantify the difference between predicted and true values, with lower values indicating higher prediction accuracy. The calculation methods for *RMSE* and *R* are as follows:

$$RMSE = \sqrt{\frac{1}{n}\sum_{i=1}^{n}(f_i - y_i)^2} \tag{20}$$

$$R = \frac{\sum_{i=1}^{n}(f_i - \bar{f})(y_i - \bar{y})}{\sqrt{\sum_{i=1}^{n}(f_i - \bar{f})^2 (y_i - \bar{y})^2}} \tag{21}$$

where f_i denotes the observed value, y_i is the predicted value by the model, and n represents the total number of sample points. $\bar{f}$ and $\bar{y}$ are the mean values of the observed and predicted data, respectively.

4. Experimental Results and Analysis

Since the soil salinity retrieved from Tianmu-1 GNSS-R data is point-based and lacks spatial continuity, it cannot intuitively reflect the spatial distribution of salinity. Therefore, in this study, the predicted results were interpolated based on their geographic coordinates to generate raster images with the same spatial resolution as SMAP data.

To evaluate the effectiveness of the proposed fusion model in soil salinity inversion, we compared it against three benchmark models: Extreme Gradient Boosting

(XGBoost), Artificial Neural Network (ANN), and a standard Transformer model. All models were trained under identical settings, and their performance on the test set was evaluated in terms of predictive accuracy and spatial representation capability. The evaluation metrics included the correlation coefficient (R) and root mean square error (RMSE), alongside an in-depth analysis of model fitting and geographic spatial expression.

Figure 2 presents the scatter plots of predicted soil salinity versus the reference values for each model. It can be observed that the predictions from the proposed model are more densely distributed around the ideal fitting line (y = x), demonstrating the strongest correlation and the fewest outliers—significantly outperforming the other three methods. In contrast, the ANN model exhibits noticeable dispersion in its predictions. While XGBoost and Transformer models show moderate improvements, systematic biases are still present.

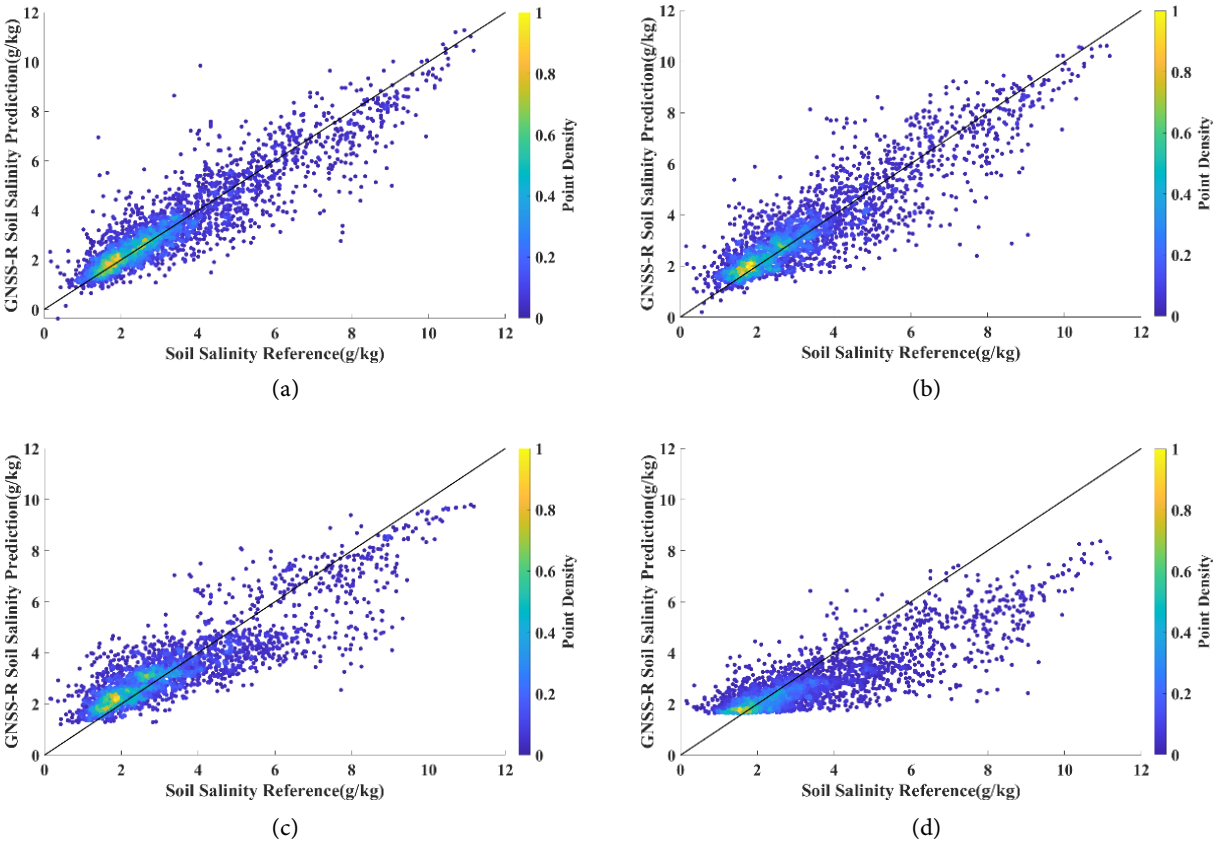

Figure 2. Scatter plot of inversion results. (a) MLF-Net; (b) Transformer; (c) XGBoost; (d) ANN.

Table 2 presents the prediction accuracy of the proposed model and three baseline models on the test dataset. The results show that the proposed MLF-Net achieves the best performance across all evaluation metrics, with a correlation coefficient (R) of 0.9137 and a root mean square error (RMSE) of 0.8050 g/kg. This significantly outperforms the other models, indicating that MLF-Net has a clear advantage in capturing complex nonlinear relationships and extracting deep seman-

tic interactions between high-dimensional image and auxiliary features.

Table 2. Accuracy evaluation table.

Evaluation indicators	MLF-Net	Transformer	XGBoost	ANN
Correlation coefficient	0.9137	0.8948	0.8758	0.8483
Root mean square error (g/kg)	0.8050	0.8902	0.9702	1.2862

Although the Transformer model possesses strong global modeling capabilities, its performance is slightly inferior to MLF-Net. The XGBoost model performs relatively well among traditional machine learning methods, but its lack of spatial structure modeling limits its overall effectiveness compared to deep learning models. The ANN model exhibits the weakest performance, with an R value of only 0.8483 and the highest RMSE of 1.2862 g/kg, highlighting its limited suitability for complex remote sensing inversion tasks.

In summary, MLF-Net demonstrates superior predictive accuracy and stability in soil salinity retrieval, indicating its strong potential for practical applications.

Figure 3 illustrates the comparison between predicted soil salinity values and reference values across 200 randomly selected samples using four models: MLF-Net, Transformer, XGBoost and ANN. The line chart shows the prediction trends, while the accompanying bar chart presents the absolute deviations between predicted and reference values for each model.

Overall, MLF-Net demonstrates the highest consistency with the reference curve, exhibiting the smallest error fluctuations and closely matching the overall trend of the observed values. This confirms the superior performance of MLF-Net

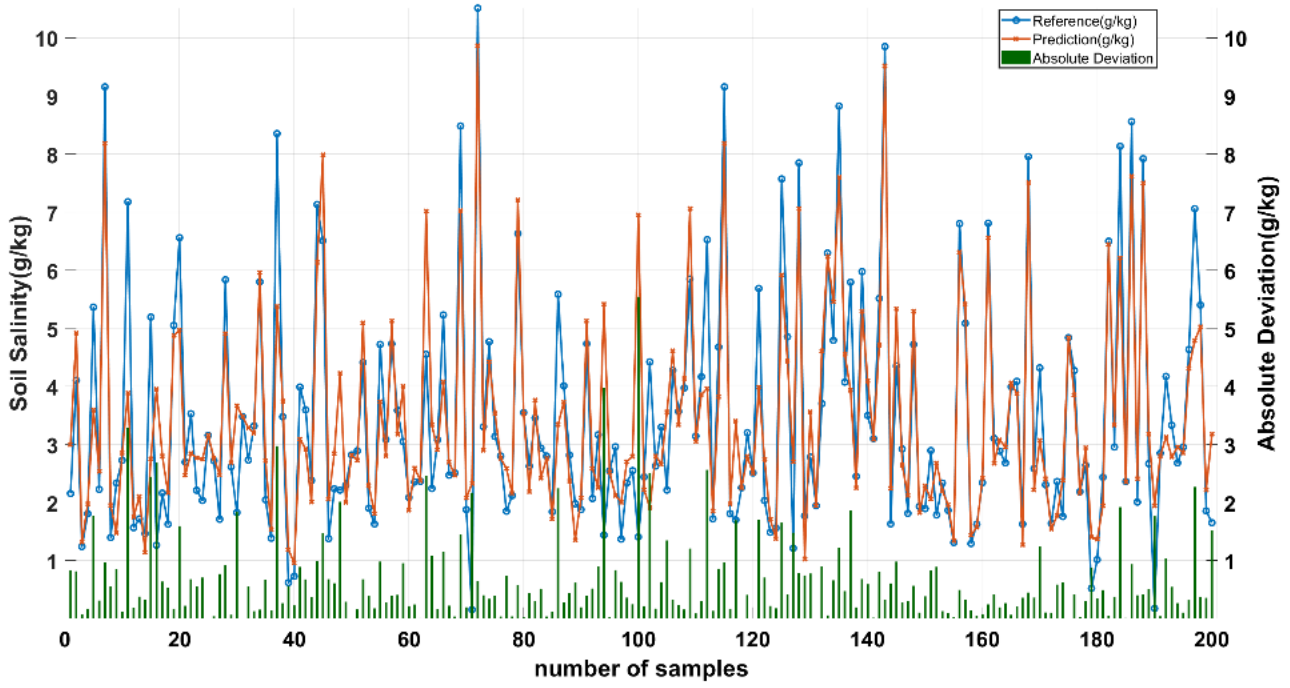

(a)

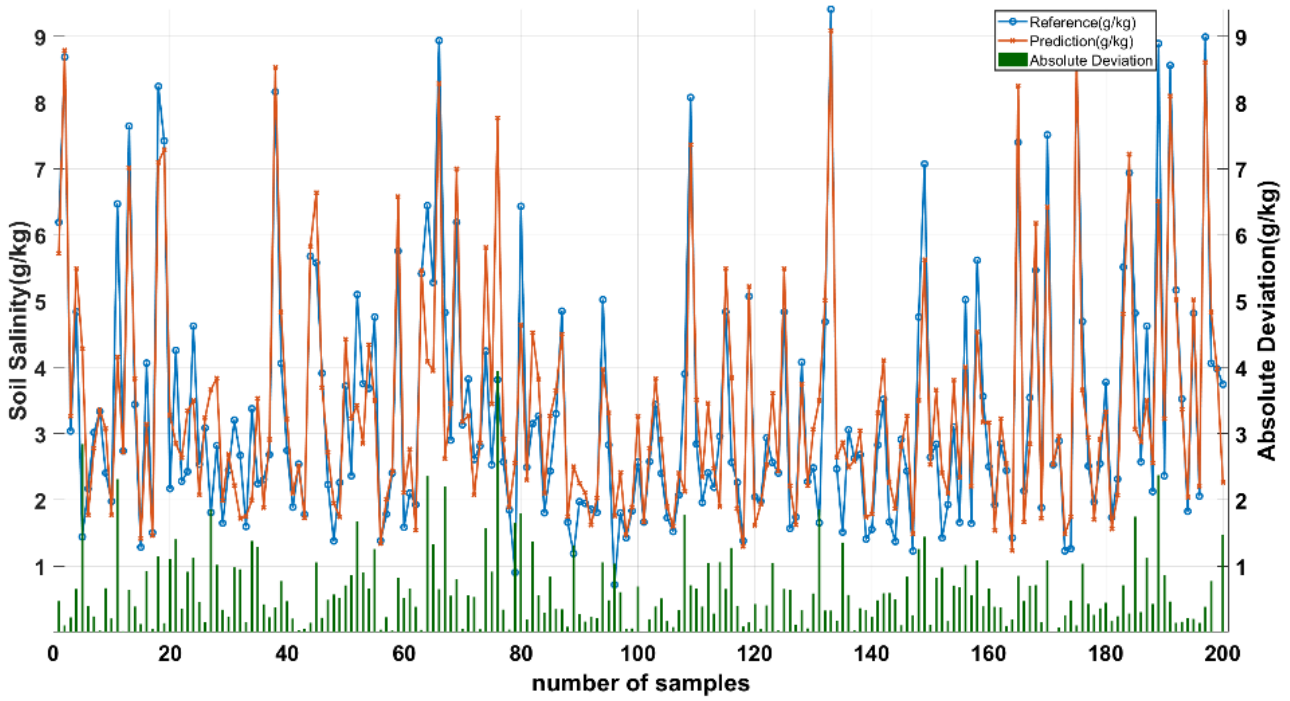
Reference(g/kg)
Prediction(g/kg)
Absolute Deviation
Soil Salinity(g/kg)
Absolute Deviation(g/kg)
number of samples
0
20
40
60
80
100
120
140
160
180
200
1
2
3
4
5
6
7
8
9

(b)

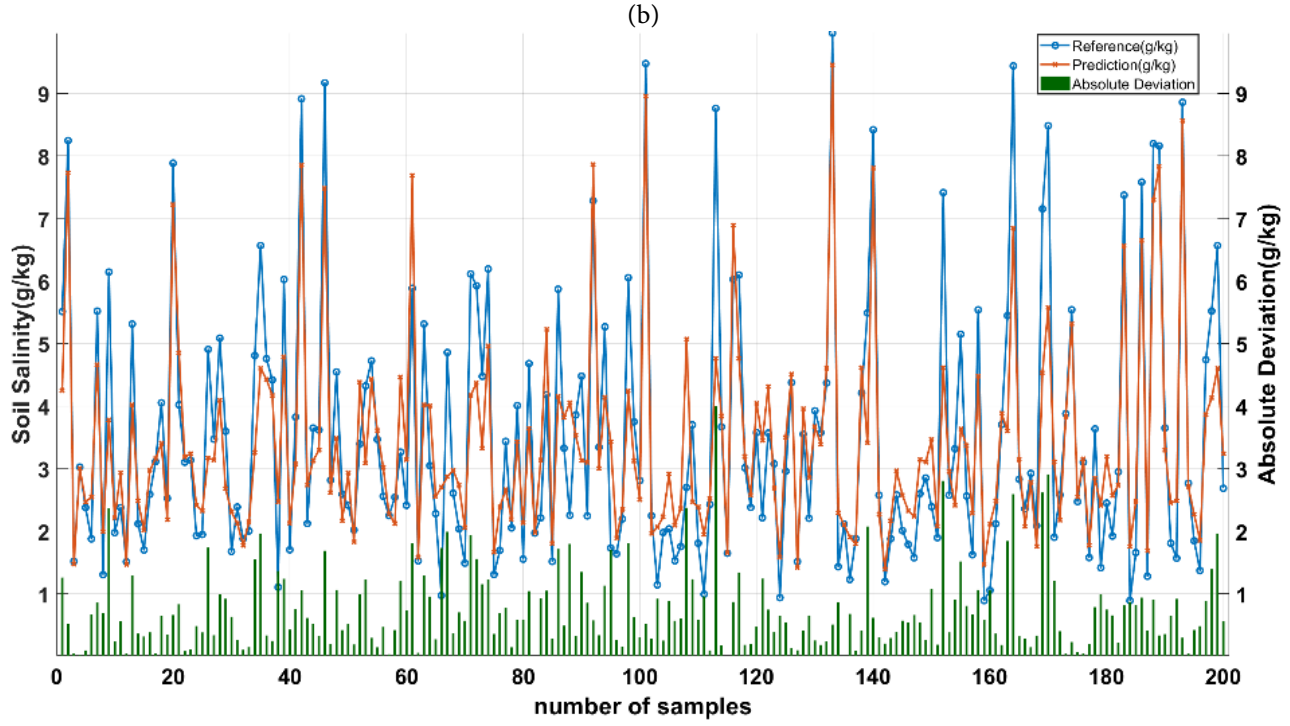
Reference(g/kg)
Prediction(g/kg)
Absolute Deviation
Soil Salinity(g/kg)
Absolute Deviation(g/kg)
number of samples
0
20
40
60
80
100
120
140
160
180
200
1
2
3
4
5
6
7
8
9

(c)

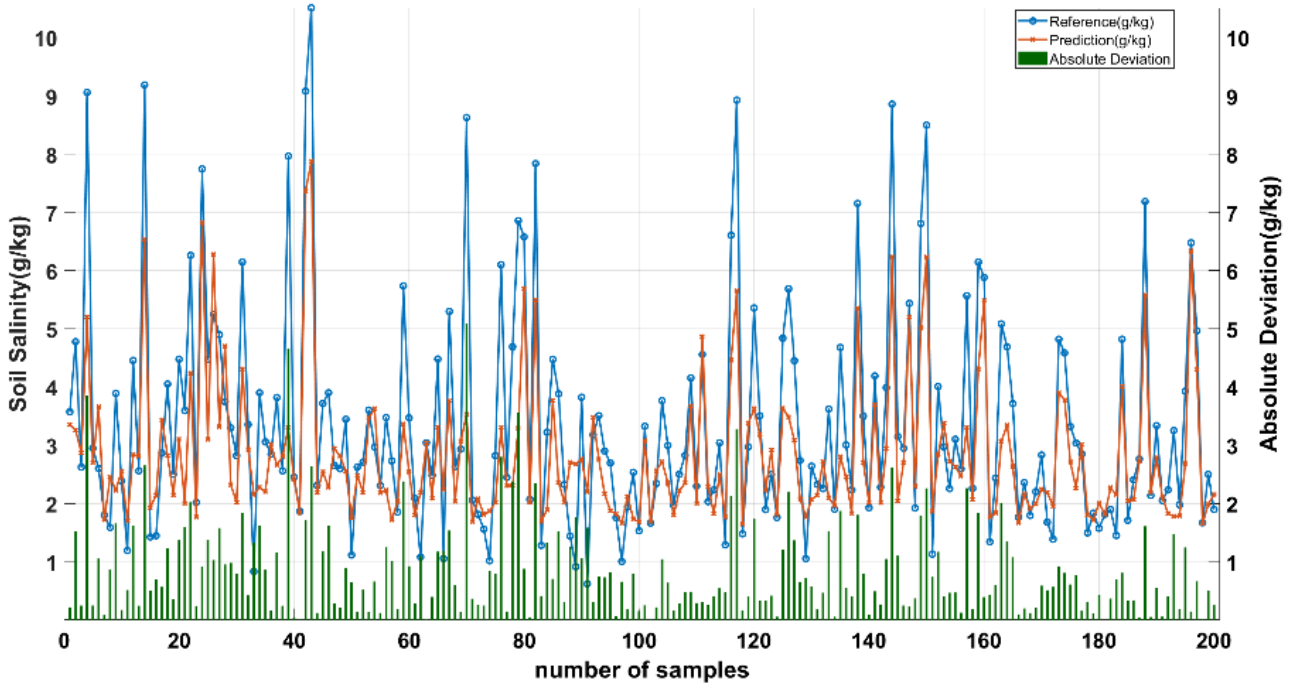

(d)

Figure 3. Line graph of inversion results. (a) MLF-Net; (b) Transformer; (c) XGBoost; (d) ANN.

in soil salinity retrieval. The Transformer model ranks second, showing generally consistent trends with the observations despite some localized deviations. XGBoost displays noticeable discrepancies in certain intervals, reflecting its limited capacity to capture complex nonlinear relationships. The ANN model performs the worst, with large fluctuations and significant prediction errors, indicating poor generalization ability.

The absolute deviation bars further validate these findings, with MLF-Net achieving the smallest prediction errors and ANN the largest. In summary, MLF-Net outperforms the other three models not only in terms of prediction accuracy but also in maintaining greater stability across individual samples.

5. Conclusions

In this study, Tianmu-1 GNSS Reflectometry (GNSS-R) data was employed as the primary data source to propose a Multimodal Low-Rank Fusion Network (MLF-Net) for soil salinity retrieval. By utilizing Delay-Doppler Map (DDM) images and surface reflectivity parameters as multimodal inputs, the proposed method integrates a low-rank constraint and fusion mechanism to enable efficient and collaborative modeling of multi-source features. Comparative experiments with Transformer, XGBoost, and conventional Artificial Neural Network (ANN) models demonstrate the superior modeling capacity and prediction accuracy of MLF-Net.

Quantitative evaluation shows that MLF-Net achieves a correlation coefficient (R) of 0.9137 and a root mean square error (RMSE) of only 0.8050 g/kg, outperforming all three benchmark models, and exhibiting enhanced prediction perfor-

mance and generalization ability. Further analyses using line plots and absolute deviation charts confirm that MLF-Net maintains low prediction errors across most samples, indicating robust stability.

In summary, the proposed MLF-Net exhibits strong overall performance in the task of soil salinity retrieval and proves suitable for large-scale remote sensing applications. It offers a promising technical solution for regional-scale soil salinity monitoring.

Funding

This work was supported by the Key Program of joint Fund of the National Natural Science Foundation of China and Shandong Province under Grant U22A20586, the Natural Science Foundation of Shandong Province under Grant ZR2022MD015, the Fundamental Research Funds for the Central Universities under Grant 24CX02030A, the National Natural Science Foundation of China under Grant 41701513, 61371189, and 41772350, and the Key Research and Development Program of Shandong Province under Grant 2019GGX101033.

Acknowledgements

We extend our sincere gratitude to NASA for the provision of SMAP data, as well as to the Tianmu Satellite team for providing the Tianmu satellite data.

Conflicts of Interest

The authors declare no conflicts of interest regarding the publication of this paper.

References

[1] Rodriguez-Alvarez, N., Monerris, A., Bosch-Lluis, X., Camps, A., Vall-Llossera, M., Marchan-Hernandez, J.F., *et al.* (2009) Soil Moisture and Vegetation Height Retrieval Using GNSS-R Techniques. 2009 *IEEE International Geoscience and Remote Sensing Symposium*, Cape Town, 12-17 July 2009, III-869-III-872. https://doi.org/10.1109/igarss.2009.5417907

[2] Li, W., Cardellach, E., Fabra, F., Ribo, S. and Rius, A. (2020) Assessment of Spaceborne GNSS-R Ocean Altimetry Performance Using CYGNSS Mission Raw Data. *IEEE Transactions on Geoscience and Remote Sensing*, **58**, 238-250. https://doi.org/10.1109/tgrs.2019.2936108

[3] Huang, F., Garrison, J.L., Rodriguez-Alvarez, N., O'Brien, A.J., Schoenfeldt, K.M., Ho, S.C., *et al.* (2019) Sequential Processing of GNSS-R Delay-Doppler Maps to Estimate the Ocean Surface Wind Field. *IEEE Transactions on Geoscience and Remote Sensing*, **57**, 10202-10217. https://doi.org/10.1109/tgrs.2019.2931847

[4] Lecun, Y., Bottou, L., Bengio, Y. and Haffner, P. (1998) Gradient-Based Learning Applied to Document Recognition. *Proceedings of the IEEE*, **86**, 2278-2324. https://doi.org/10.1109/5.726791

[5] Vaswani, A., Shazeer, N., Parmar, N., Uszkoreit, J., Jones, L., Gomez, A.N., Kaiser, Ł. and Polosukhin, I. (2017) Attention Is All You Need. *Proceedings of the* 31*st International Conference on Neural Information Processing Systems*, Long Beach, 4-9 December 2017, 6000-6010.

[6] Hou, H.H., Wang, C.T., Wang, X.D. and Gao, F.H. (2014) A Study of Improvement Effects by Biological Measures in the Yellow River Delta Saline-Alkali Soil. *China Rural Water and Hydropower*, No. 7, 1-6. (In Chinese)

[7] Chunli, B.A.I. (2020) Scientific and Technological Innovation Leads High-Quality Development of Agriculture in the Yellow River Delta. *Bulletin of Chinese Academy of Sciences* (*Chinese Version*), **35**, 138-144. (In Chinese)

[8] Liu, X., Bu, J., Zuo, X., Wang, Z., Wang, Q., Wang, Q., *et al.* (2025) Performance Validation of Sea Surface Wind Speed Retrieval Algorithms and Products from the Chinese Tianmu-1 Constellation GNSS-R: First Results on Comparison with Other Wind Speed Products. *IEEE Journal of Selected Topics in Applied Earth Observations and Remote Sensing*, **18**, 5189-5203. https://doi.org/10.1109/jstars.2025.3527026

[9] Fischer, G., Nachtergaele, F., Prieler, S., van Velthuizen, H.T., Verelst, L. and Wiberg, D. (2008) Global Agro-Ecological Zones Assessment for Agriculture (GAEZ 2008). IIASA, FAO.

[10] O'Neill, P., Chan, S., Njoku, E.G., Jackson, T. and Bindlish, R. (2018) Algorithm Theoretical Basis Document Level 2 & 3 Soil Moisture (Passive) Data Products. Jet Propulsion Laboratory.

[11] Bindlish, R. and Barros, A.P. (2001) Parameterization of Vegetation Backscatter in Radar-Based, Soil Moisture Estimation. *Remote Sensing of Environment*, **76**, 130-137. https://doi.org/10.1016/s0034-4257(00)00200-5

[12] Dai, S., Song, D. and Wang, B. (2025) CT-NET: A Cross-Modal Transformer Network for Satellite-Borne GNSS-R Soil Moisture Retrieval. *International Conference on Remote Sensing and Digital Earth* (*RSDE* 2024), Volume 13514, 135140S. https://doi.org/10.1117/12.3059047

[13] Wang, J.R. and Schmugge, T.J. (1980) An Empirical Model for the Complex Dielectric Permittivity of Soils as a Function of Water Content. *IEEE Transactions on Geoscience and Remote Sensing*, **18**, 288-295. https://doi.org/10.1109/tgrs.1980.350304

[14] Hu, Q.R. (2003) Studies on Microwave Dielectric Behavior of Moist Salt Soil and Its Effect on Backscattering Coefficients Extracted from Radar Image. Ph.D. Thesis, Chinese Academy of Sciences, Institute of Remote Sensing Applications. (In Chinese)